

Two-fluid modelling of the desulphurisation process within a bubbling fluidised bed coal gasifier

L.M. Armstrong[†], S. Gu^{*‡}, K.H. Luo^{†*}

[†]Energy Technology Research Group, University of Southampton, Southampton, SO17 1BJ, UK

[‡]School of Engineering, Cranfield University, Cranfield, Bedfordshire, MK43 0AL, UK

^{*}Centre for Combustion Energy, Key Laboratory for Thermal Science and Power Engineering of Ministry of Education, Department of Thermal Engineering, Tsinghua University, Beijing 100084, China

^{*}Email: s.gu@cranfield.ac.uk

Abstract

The present work introduces the desulphurisation process to a two- and three-dimensional Eulerian-Eulerian CFD model of a coal bubbling fluidised gasifier. The desulphurisation process is important for the reduction of harmful SO_x emissions, therefore the development of a CFD model capable of predicting chemical reactions involving desulphurisation is key to the optimisation of reactor designs and operating conditions. To model the process, one gaseous phase and five particulate phases are included. Devolatilisation, heterogeneous and homogeneous chemical reactions as well as calcination and desulphurisation reactions are incorporated. A calcination-only model and a calcination plus desulphurisation model are simulated in two and three dimensions and the concentrations of SO₂ leaving the reactors are compared. The simulated results are assessed against available published experimental data. The influence of the fluidised bed on the desulphurisation is also considered.

Introduction

Fluidised beds technologies (FBT) offer higher efficiencies over fixed bed technologies as the fuel particles are suspended and mixed thoroughly allowing for good air-particle contact. The particles are small so the reaction rates are fast and the good mixing allows for complete carbon removal.

Computational fluid dynamic (CFD) is increasingly used for simulating the complex gas-solid flow processes that take place in FBT. Isothermal hydrodynamics modelling of fluidised beds has been used to enhance the understanding of complex interactions between gas and particles¹⁻⁶. Computational models predicting the heat-transfer coefficient in bubbling fluidised beds have also been considered⁷⁻¹⁰.

For hydrodynamic and heat transfer, the Eulerian-Eulerian two-fluid model (TFM) is the most frequently applied method as it is less computationally exhaustive in comparison to the Eulerian-Lagrangian discrete method which simulates the individual particle dynamics compared to the TFM assumes the gas and solid

phases as continuous and fully interpenetrating within each control volume. Interesting alternatives include a Lagrangian-Lagrangian approach^{11–13} and a combination of the Eulerian-Eulerian continuum model and the Eulerian-Lagrangian discrete model^{14,15}. However these were limited to the number of particles due to computational costs. The multi-phase-particle-in-cell (MP-PIC) method is a hybrid method where particle properties are mapped to and from an Eulerian grid using interpolation functions¹⁶. A recent applications of this model include isothermal cases¹⁷ and heat transport and chemical cases, including pyrolysis^{18,19}.

The particulate phases are treated as a fluid with closure models accounting for particulate behaviours. The kinetic theory of granular flow (KTGF) is adopted to consider the particle motion. During random particle oscillations, inelastic collisions occur which dissipates energy. The granular temperature defines the average of the three variances of the particle’s velocities due to these oscillations. A full mathematical description of the kinetic theory is provided in the literature²⁰.

Reaction modelling is a recent development for simulating the gasification processes within fluidised beds, and is still limited in scope due to the high computational cost. However, the increase in computer performance and capabilities in recent years allows for such complex models to be carried out. A two-dimensional Eulerian-Eulerian model of the gasification of Colombian coal was carried out²¹ based on the experimental work from the literature²². Their model included the devolatilisation, heterogeneous reactions and homogeneous reactions and produced reasonable results. Their work was further extended to three-dimensions²³, also obtaining reasonable results. However, their models considered a single solid phase for the coal and sand which is computationally more efficient but unrealistic, as different solid materials exhibit different material properties, e.g., density, diameter, etc. Separate phases for different solid phases have been carried out^{24–26} and it was found that the use of multiple phases better represented the segregative tendencies of the bed due to different material properties.

Limestone calcination has been considered in fluidisation modelling (FM)^{27,28}; however, regardless of the multiphase flow dynamics being considered using semi-empirical fluid-dynamic correlations, the model does not consider the complex gas-particle dynamics that are present. We previously introduced limestone calcination to an Eulerian-Eulerian CFD calculation^{25,26}.

The release of SO_x and NO_x species, despite their low concentrations, is causing environmental problems. It is important to understand the factors that influence the production of such species, especially sulphur dioxide, SO_2 . Several investigations have been performed on the detection of SO_x , NO_x and the intermediates of their formations^{29–31}. Several models have been performed to determine the release of low concentration species during the devolatilisation process^{32,33} and also their inclusion in numerical models^{30,32,34}. There are many factors that can affect the production of both SO_x and NO_x species including operating conditions and sorbents, such as limestone. Since Eulerian-Eulerian models have successfully been attempted to demonstrate the effects such modification have on the gasification processes in bubbling fluidised beds it is important to

use this type of modelling to expand into the regions of low concentration modelling. Understanding the effects of low concentration species such as SO_2 , not only on the reactive behaviours within the bed and flow dynamics but also on the computational performance, is a stepping stone towards the inclusion of further low concentration species, namely their formation intermediates, which would then lead to a more realistic treatment of complex reactions.

The present work incorporates desulphurisation modelling into the Eulerian-Eulerian TFM using multiple phases for coal, char, calcium carbonate (CaCO_3), calcium oxide (CaO) and calcium sulphate (CaSO_4). The desulphurisation process, to the author’s knowledge, has yet to be included in the Eulerian-Eulerian modelling of a bubbling fluidised bed gasifier. In order to incorporate the desulphurisation process additional gas species and reactions are required for species of much lower concentrations compared to those considered previously. The present work shows the influences such additions have on the computational performance, which has yet to be demonstrated, and is important before advanced devolatilisation schemes can be considered. The effects of the concentration species on exiting emissions and the influence bed dynamics have on them are also considered.

Model Setup

The present numerical study includes five phases: one gaseous phase and five particulate phases, char, coal, CaCO_3 , CaO and CaSO_4 , within a fluidised bed with experimental measurements taken from the literature²². This model was chosen over the Eulerian-Lagrangian models as it is computationally more efficient in terms of computational time and memory. The commercial software ANSYS 12.0 was used to simulate the multiphase model using the Eulerian-Eulerian Two-Fluid model (TFM). The TFM allows for the presence of multiple phases in one control volume by introducing the volume fraction variable, α_i . Each of the solid phases restricts the granular particles to the same diameter and density as the properties are averaged over the control volumes and solved individually using the mass and momentum equations. The kinetic fluctuations between particles are considered using the kinetic theory of granular flow. The virtual mass and lift effects are negligible as the lift only affects particles of large diameters and this is not the present case.

Conservation of Mass

The conservation of mass for the gaseous and solid phases are modelled using the following equations:

$$\frac{\partial (\alpha_g \rho_g)}{\partial t} + \nabla \cdot (\alpha_g \rho_g \vec{v}_g) = S_{gs} \quad (1)$$

$$\frac{\partial (\alpha_s \rho_s)}{\partial t} + \nabla \cdot (\alpha_s \rho_s \vec{v}_s) = S_{sg} \quad (2)$$

$$S_{sg} = -S_{gs} = w_i \Sigma Y_i R_i \quad (3)$$

where \vec{v}_i and ρ_i represent the instantaneous velocity of the phase and density, respectively. A mass source term is introduced due to the mass, momentum and heat exchange between the gaseous and solid phases as a result of the heterogeneous reactions. The gas density, ρ_g , is defined as a function of species composition and temperature using the ideal gas law whilst the solid density, ρ_s , is defined by the composition of the species alone.

$$\rho_g = \frac{p}{RT \Sigma_{i=1}^n \frac{Y_i}{w_i}} \quad (4)$$

$$\rho_s = \frac{1}{\Sigma_{i=1}^n \frac{Y_i}{\rho_i}} \quad (5)$$

Conservation of Momentum

The conservation of momentum equation for the gas and solid phases are given as follows:

$$\frac{\partial (\alpha_g \rho_g \vec{v}_g)}{\partial t} + \nabla \cdot (\alpha_g \rho_g (\vec{v}_g \otimes \vec{v}_g)) = -\alpha_g \nabla p + \nabla \cdot \bar{\bar{\tau}}_g + \alpha_g \rho_g \vec{g} + K_{gs} (\vec{v}_g - \vec{v}_s) + S_{gs} \vec{v}_s \quad (6)$$

$$\frac{\partial (\alpha_s \rho_s \vec{v}_s)}{\partial t} + \nabla \cdot (\alpha_s \rho_s (\vec{v}_s \otimes \vec{v}_s)) = -\alpha_s \nabla p - \nabla p_s + \nabla \cdot \bar{\bar{\tau}}_s + \alpha_s \rho_s \vec{g} + K_{gs} (\vec{v}_g - \vec{v}_s) + S_{sg} \vec{v}_s \quad (7)$$

where K_{gs} and $\bar{\bar{\tau}}$ represent the interphase momentum transfer between the phases and the stress strain tensor, respectively. The stress-strain tensors for the separate phases are given by:

$$\bar{\bar{\tau}}_g = \alpha_g \mu_g (\nabla \vec{v}_g + \nabla \vec{v}_g^T) - \frac{2}{3} \alpha_g \mu_g (\nabla \cdot \vec{v}_g) \bar{\bar{I}}_g \quad (8)$$

$$\bar{\bar{\tau}}_s = \alpha_s \mu_s (\nabla \vec{v}_s + \nabla \vec{v}_s^T) + \alpha_s \left(\xi_s - \frac{2}{3} \mu_s \right) \nabla \cdot \vec{v}_s \quad (9)$$

where the bulk viscosity, ξ_s , accounts for the resistance of the particle to expansion and compression³⁵. The gas viscosity, μ_g is made of the gas phase laminar viscosity and the gas phase turbulent viscosity:

$$\xi_s = \frac{4}{3}\alpha_s d_s \rho_s g_0 (1+e) \left(\frac{\Theta_s}{\pi}\right)^{1/2} \quad (10)$$

$$\mu_g = \mu_{gl} + \mu_{gt} \quad (11)$$

The solid shear viscosity is composed of collisional, kinetic and frictional effects. For the collisional and kinetic effects the coefficient of restitution was introduced to account for the loss of energy due to particle collisions³⁶. The coefficient quantifies the elasticity of the particle collisions where a value of 0 is fully inelastic collisions whilst a coefficient of 1 is a fully elastic collisions. Schaeffer's expression³⁷ is used to model the frictional viscosity in dense cases.

$$\mu_s = \mu_{s_{col}} + \mu_{s_{kin}} + \mu_{s_{fr}} \quad (12)$$

$$\mu_{s_{col}} = \frac{4}{5}\alpha_s d_s \rho_s g_0 (1+e) \left(\frac{\Theta_s}{\pi}\right)^{1/2} \quad (13)$$

$$\mu_{s_{kin}} = \frac{10d_s \rho_s \sqrt{\Theta_s \pi}}{96\alpha_s (1+e) g_0} \left[1 + \frac{4}{5}\alpha_s g_0 (1+e)\right]^2 \quad (14)$$

$$\mu_{s_{fr}} = \frac{p_s \sin\phi}{2\sqrt{I_{2D}}} \quad (15)$$

The solids pressure considers the kinetic effects and the effects due to particle collisions, and g_0 represents the radial distribution function which modifies the probability of particle collisions as the phase becomes dense:

$$p_s = \alpha_s \rho_s \Theta_s + 2\rho_s (1+e) \alpha_s^2 g_0 \Theta_s \quad (16)$$

$$g_0 = \left[1 - \left(\frac{\alpha_s}{\alpha_{s_{max}}}\right)^{1/3}\right]^{-1} \quad (17)$$

The drag models represent the interphase momentum transfer between the gas and particle phases. The Gidaspow model³⁸ is a combination of the Wen and Yu model for dilute phases³⁹ and the Ergun model for dense phases⁴⁰:

$$K_{gs} = \begin{cases} 150 \frac{\alpha_s^2 \mu_g}{\alpha_g d_s^2} + 1.75 \frac{\alpha_s \rho_g |\vec{v}_g - \vec{v}_s|}{d_s} & \text{for } \alpha_g \leq 0.8; \\ \frac{3}{4} C_D \frac{\alpha_g \rho_g |\vec{v}_g - \vec{v}_s|}{d_s} \alpha_g^{-2.65} & \text{for } \alpha_g > 0.8. \end{cases} \quad (18)$$

$$C_D = \begin{cases} \frac{24}{Re_s} [1 + 0.15 Re_s^{0.687}] & \text{if } Re_s \leq 1000; \\ 0.44 & \text{if } Re_s > 1000. \end{cases} \quad (19)$$

$$Re_s = \frac{\rho_g \alpha_g d_s |\vec{v}_g - \vec{v}_s|}{\mu_g} \quad (20)$$

The interphase exchange coefficient between the two solid phases, namely limestone, s_1 , and coal, s_2 , was derived by Syamlal et al.⁴¹:

$$K_{s_1 s_2} = \frac{3(1+e) \left(\frac{\pi}{2}\right) \alpha_{s_1} \alpha_{s_2} \rho_{s_1} \rho_{s_2} (d_{s_1} + d_{s_2})^2 g_0}{2\pi (\rho_{s_1} d_{s_1}^3 + \rho_{s_2} d_{s_2}^3)} \left| \vec{v}_{s_1} - \vec{v}_{s_2} \right| \quad (21)$$

Gas Turbulence Model

The $k - \epsilon$ turbulence model is used to model the gaseous phase only. The solid phases are considered laminar due to the influence of drag in the bubbling bed dominating the solid flow behaviour. The turbulent mixing rate and chemical kinetic rates are calculated for the finite-rate/eddy-dissipation homogeneous reaction model therefore it is important to consider a turbulent model for the gas phase. The transport equations for k and ϵ are as follows:

$$\frac{\partial (\alpha_g \rho_g k)}{\partial t} + \nabla \cdot (\alpha_g \rho_g \vec{v}_g k) = \nabla \cdot \alpha_g \left(\mu_{gt} + \frac{\mu_{gt}}{\sigma_k} \nabla \cdot k \right) + \alpha_g G_k - \alpha_g \rho_g \epsilon \quad (22)$$

$$\frac{\partial (\alpha_g \rho_g \epsilon)}{\partial t} + \nabla \cdot (\alpha_g \rho_g \vec{v}_g \epsilon) = \nabla \cdot \alpha_g \left(\mu_{gt} + \frac{\mu_{gt}}{\sigma_\epsilon} \nabla \cdot \epsilon \right) + \frac{\alpha_g \epsilon}{\kappa} (C_{\epsilon_1} G_\kappa - C_{\epsilon_2} \rho_g \epsilon) \quad (23)$$

$$\mu_{gt} = \rho_g C_\mu \frac{k^2}{\epsilon} \quad (24)$$

Equation 24 defines the turbulence viscosity used in Equation 9. The model constants are $C_{\epsilon_1} = 1.44$, $C_{\epsilon_2} = 1.92$ and $C_\mu = 0.09$. The turbulent Prandtl numbers for k and ϵ are $\sigma_k = 1.0$ and $\sigma_\epsilon = 1.3$, respectively. G_k represents the generation of turbulent kinetic energy due to the mean velocity gradients and is represented by:

$$G_k = -\rho_g \overline{v'_i v'_j} \frac{\partial v_j}{\partial x_i} \quad (25)$$

where

$$-\rho_g \overline{v'_i v'_j} = \mu_{gt} \left(\frac{\partial v_i}{\partial x_j} + \frac{\partial v_j}{\partial x_i} \right) - \frac{2}{3} \rho_g k \delta_{ij} \quad (26)$$

Kinetic Theory of Granular Flow

The granular temperature of the solid phases, Θ_s , is proportional to the kinetic energy of the random fluctuating motion of the particles. The following equation is solved for the granular temperature:

$$\frac{3}{2} \left[\frac{\partial}{\partial t} (\alpha_s \rho_s \Theta_s) + \nabla \cdot (\alpha_s \rho_s \vec{v}_s \Theta_s) \right] = \left(-p_s \cdot \bar{\vec{I}} + \bar{\vec{\tau}}_s \right) : \nabla \vec{v}_s - \gamma_{\Theta_s} + \nabla \cdot (k_{\Theta_s} \cdot \nabla \Theta_s) - 3K_{gs} \Theta_s \quad (27)$$

The diffusion coefficient, k_{Θ_s} , and collisional dissipation, γ_{Θ_s} , are given by:

$$k_{\Theta_s} = \frac{150 \rho_s d_s \sqrt{\Theta_s \pi}}{384 (1+e) g_0} \left[1 + \frac{6}{5} \alpha_s g_0 (1+e) \right]^2 + 2 \alpha_s^2 \rho_s d_s (1+e) g_0 \sqrt{\frac{\Theta_s}{\pi}} \quad (28)$$

$$\gamma_{\Theta_s} = \frac{12 (1-e)^2 g_0}{d_s \sqrt{\pi}} \alpha_s^2 \rho_s \Theta_s^{3/2} \quad (29)$$

Conservation of Energy

The conservation of energy considers the heat transfer within each phase and the exchange of heat between different phases. Each phase has a separate enthalpy equation and determined by the specific enthalpy, H , the thermal conductivity, λ_i , and the heat exchange between the gas and solid phases, Q_{gs} , as follows:

$$\frac{\partial}{\partial t} (\alpha_g \rho_g H_g) + \nabla \cdot (\alpha_g \rho_g \vec{v}_g H_g) = \nabla (\lambda_g \nabla T_g) + Q_{gs} + S_{gs} H_s \quad (30)$$

$$\frac{\partial}{\partial t} (\alpha_s \rho_s H_s) + \nabla \cdot (\alpha_s \rho_s \vec{v}_s H_s) = \nabla (\lambda_s \nabla T_s) + Q_{sg} + S_{sg} H_s \quad (31)$$

$$H_s = \sum_j Y_i H_i \quad (32)$$

$$H_i = \int_{T_0}^T C_{p,i} dT + \Delta H_{f,i} \quad (33)$$

$$\lambda_g = \sum_j \frac{X_j \lambda_j}{\sum_j X_j \phi_{ij}} \quad (34)$$

where H_s represents the source term that includes sources of enthalpy, H_i is the enthalpy for each species in the mixture and λ_g is the gas mixture thermal conductivity.

In Equation 34, X_i represents the molar fraction of the i^{th} species and

$$\phi_{ij} = \left[1 + \left(\frac{\mu_i}{\mu_j} \right)^{1/2} \left(\frac{w_i}{w_j} \right)^{1/4} \right] / \left[8 \left(1 + \frac{w_i}{w_j} \right) \right]^{1/2}.$$

The heat exchange between the phases, Q_{gs} , is a function of temperature difference and given by:

$$Q_{gs} = -Q_{sg} = h_{gs} (T_g - T_s) \quad (35)$$

An empirical relation for the interphase heat transfer coefficient between the gaseous and solid phases was proposed⁴² which relates the Nusselt number with the particle Reynolds and the Prandtl numbers, $Pr = \frac{C_{p,g}\mu_g}{\kappa_g}$:

$$Nu_s = (7 - 10\alpha_g + 5\alpha_g^2)[1 + 0.7(Re_p)^{0.2}(Pr)^{1/3}] + (1.33 - 2.40\alpha_g + 1.20\alpha_g^2)(Re_p)^{0.2}(Pr)^{1/3} \quad (36)$$

Species Transport Equations

The mass fraction of each species in the gas phase, Y_i is determined from the conservation equation of species transport as follows:

$$\frac{\partial}{\partial t}(\alpha_g \rho_g Y_i) + \nabla(\alpha_g \rho_g \vec{v}_g Y_i) = -\nabla \cdot \alpha_g J_i + \alpha_g R_{g,i} + R_{s,i} \quad (37)$$

$$J_i = -\left(\rho_g D_{m,i} + \frac{\mu_t}{Sc_t}\right) \nabla Y_i \quad (38)$$

$$D_{m,i} = \frac{1 - X_i}{\sum_{j \neq i} \frac{X_j}{D_{i,j}}} \quad (39)$$

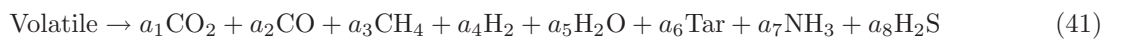
The second and third terms on the right hand side of Equation 37 represent the homogeneous rate of production of species, i , and the heterogeneous rate of reaction, respectively. J_i is the diffusion flux of the individual species, i , as a results of concentration gradients and is calculated using the modified Fick's law for the diffusion flux of chemical species in turbulent flow. Sc_t is the turbulent Schmidt number which is set to 0.7, and $D_{m,i}$ is the mixture diffusion coefficients.

Reaction Modelling

The present work considers 1) the coal devolatilisation modelling; 2) heterogeneous char reactions, 3) homogeneous gaseous reactions, 4) limestone calcination and 5) desulphurisation. The heterogeneous, homogeneous, calcination and desulphurisation reactions that take place are given in Table 1.

Devolatilisation

During the devolatilisation process, the coal phase immediately transfers the char into the char phase whilst the gaseous volatiles are released. For simplicity the coal is assumed dry and ash free so the presence of ash is neglected in the present case. However, we are currently investigating the presence of ash with more complex reaction models.



The mass fraction, Y_i of the dominating volatile products released during devolatilisation are determined using correlations that estimate the yields by the proximate analysis⁴³, given in Table 2, as follows:

$$Y_{CO_2} = 0.135 - 0.900Y_{\text{volatile(daf)}} + 1.906Y_{\text{volatile(daf)}}^2 \quad (42)$$

$$Y_{CO} = 0.428 - 2.653Y_{\text{volatile(daf)}} + 4.845Y_{\text{volatile(daf)}}^2 \quad (43)$$

$$Y_{CH_4} = 0.201 - 0.469Y_{\text{volatile(daf)}} + 0.241Y_{\text{volatile(daf)}}^2 \quad (44)$$

$$Y_{H_2} = 0.157 - 0.868Y_{\text{volatile(daf)}} + 1.388Y_{\text{volatile(daf)}}^2 \quad (45)$$

$$Y_{H_2O} = 0.409 - 2.389Y_{\text{volatile(daf)}} + 4.554Y_{\text{volatile(daf)}}^2 \quad (46)$$

$$Y_{Tar} = -0.325 + 7.279Y_{\text{volatile(daf)}} - 12.880Y_{\text{volatile(daf)}}^2 \quad (47)$$

The volatile nitrogen and sulphur species are determined as a function of bed temperature, T ,⁴⁴:

$$N = 0.001T - 0.6 \quad (kg/kg \text{ coal}) \quad (48)$$

$$S = 0.001T - 0.06 \quad (kg/kg \text{ coal}) \quad (49)$$

Heterogeneous Reactions

Heterogeneous reactions take place between the char and the surrounding gases. The char combustion between the char and O_2 takes place very quickly. The reactions take place on the external surface of the particles therefore models have been created that consider the kinetic, $K - Arr$, and the diffusive, $K - Dif$, rate constants as follows:

$$R_C = \left((K_{Arr})^{-1} + (K_{Dif})^{-1} \right) C_{O_2} \quad (50)$$

$$K_{Arr} = AT_s^n \exp \left(\frac{E}{RT_s} \right) \quad (51)$$

$$K_{Dif} = \frac{Sh D_{gs} w_C}{RT_s d_s} \quad (52)$$

$$Sh = 2.0 + 0.6 Re^{1/2} Pr^{1/3} \quad (53)$$

$$D_{gs} = \frac{8.34 \times 10^{-6} T^{1.75}}{p} \quad (54)$$

where Sh and D_{gs} are the Sherwood number and diffusion coefficient for the gas, respectively; C_{O_2} is the concentration of O_2 ; Re and Pr are the Reynolds and the Prandtl numbers, respectively; and A and E are the pre-exponential factors and activation energy, respectively.

The gasification heterogeneous reactions take place much slower than the combustion reaction and have a longer residence time within the bed. As a result, the reaction is not limited to only the external surface of the

particle therefore the consideration of diffusion through the external surface does not need to be considered:

$$R_C = K_{Arr}[C_g] \quad (55)$$

The kinetic rate constants ($\text{kgm}^{-3}\text{s}^{-1}$)^{45,46} are provided in Table 1.

Homogeneous Reactions

The homogeneous reactions within the gaseous phase consider the effects of turbulent flow and chemical reactions. The kinetic rate constant, R_{Arr} , and the turbulent mixing rate constant, R_{Edd} , were calculated using the finite-rate/eddy-dissipation model within ANSYS 12.0. The minimum of these two rates is then taken to be the net reaction rate.

$$R_{i,r} = \min(R_{Arr}, R_{Edd}) \quad (56)$$

$$R_{Arr} = k_a T^z C_A^n C_B^m \quad (57)$$

$$R_{Edd} = 4.0 v'_{i,r} w_i \rho_g \frac{\varepsilon}{\kappa} \min \left[\min_R \left(\frac{Y_R}{v'_{R,r} w_R} \right), \frac{\Sigma_P Y_P}{2 \Sigma_j^N v''_{j,r} w_j} \right] \quad (58)$$

where w_i is the species molecular weight and $v'_{i,r}$ and $v''_{j,r}$ are the stoichiometric coefficients. The homogeneous reactions with their kinetic rates ($\text{kgm}^{-3}\text{s}^{-1}$)^{28,47} are provided in Table 1.

The Calcination Process

Limestone calcination is the breakdown of limestone, CaCO_3 , into calcium oxide, CaO , and carbon dioxide, CO_2 . The reaction proceeds only if the partial pressure of CO_2 is above the decomposition pressure of CaCO_3 . The following equilibrium decomposition pressure⁴⁸ is used:

$$P_{eq} = 4.137 \times 10^7 \exp(-20474/T_l) \quad (59)$$

The calcination rate proposed by Silcox et al.⁴⁸ is dependent on the temperature and partial pressures of CO_2 and is measured in $\text{mol m}^{-2}\text{s}^{-1}$. Table 1 gives the reaction kinetics for K_{cal} :

$$R_{CAL} = K_{cal} (P_{eq} - P_i) \quad (60)$$

There are several kinetic rates available for the limestone calcination process which range in complexity. This model does not account for the particle shrinkage or sintering effects as the Eulerian-Eulerian model is restricted to same size diameters for the CaCO_3 phase, etc. A review of the calcination models and their complexities is available in the literature⁴⁹.

The Desulphurisation Process

The present work introduces the desulphurisation reaction where CaO produced during the calcination process reacts with SO₂, and O₂, to produce CaSO₄. The sulphation process only takes place in the outer layer of the CaO particle and stops once the pores become blocked with CaSO₄. An unreacted-core model was taken from the literature⁵⁰ which takes into account temperature, limestone reactivity, particle size and gas concentrations. As with the calcination model, the particulate phase diameters will remain constant as a restriction of the Eulerian-Eulerian model.

$$R_D = (\pi/6) d_{CaO}^3 K_{ds} C_{SO_2} \quad (61)$$

$$S_g = -384T_g + 5.6 \times 10^4, \quad T_g \geq 1253 \text{ K} \quad (62)$$

$$S_g = 35.9T_g - 3.67 \times 10^4, \quad T_g < 1253 \text{ K} \quad (63)$$

Initial and Boundary Conditions

The model was set up according to an experimental study of Colombian coal²². Figure 1 displays a sketch of the model set up used. The reactor had an internal diameter of 0.22 m and height of 2.0 m with a screw-feeder located at 0.3 m for the introduction of the coal and CaCO₃ mixture. An initial bed of calcium carbonate, CaCO₃ and char was set to the height of 1.0m with a volume fraction of 0.48; an equal volume fraction was used for the two solid phases of 0.24 each. The diameter of the three limestone phases, namely, CaCO₃, CaO and CaSO₄, have the same diameters but the densities vary according to the individual limestone constituent. The char is given as slightly smaller in diameter to the coal to allow for slight shrinkage following the devolatilisation process. The initial gas composition was pure nitrogen, N₂ to prevent unwanted fast oxidation reactions taking place higher up the bed and the pressure outlet was fixed to an atmosphere. A more extensive description of the operating conditions can be found from the literature²² but an overview of the present operating conditions and experimental results are given in Table 3.

The 2D and 3D meshes consisted of 2215 and 66243 cells, respectively. As performed previously^{21,25,26,51}, the cell size in the horizontal direction was 0.01 m whilst the vertical direction was set to 0.02 m creating a domain of (22 x100) cells. The region near the coal inlet was refined further to capture the devolatilisation characteristics taking place. The wall boundary conditions for the gas phase was set to no-slip whilst the particulate phase had a tangential slip condition⁵².

Both the 2D and 3D simulations utilise six separate phases, a gaseous phase and five solid phases: coal, char, CaCO₃, CaO, and CaSO₄. In order to activate the desulphurisation reaction, additional low concentration species are required. The 2D simulations consider the effects these low concentration species and additional reactions have on the computational time. The base case, which was considered in our previous

work^{25,26}, implements a gaseous mixture of 8 species, namely, H_2O , O_2 , CO_2 , CO , H_2 , CH_4 , tar and N_2 . As carried out by previous researchers^{21,53}, the tar is regarded as C_6H_6 since the composition of tar is usually regarded as condensed nuclei aromatics. The cases are extended to determine the effects of additional gaseous species, NH_3 and H_2S alone on the computational time and also the addition of two homogeneous reactions and the products of such reactions, i.e., NO and SO_2 . Table 4 contains information about the three different cases with the various species and reactions considered.

Results

Effects on computational performance

The composition of the main exiting gases, set up with cases 1, 2 and 3, were averaged over a 50.0 s period, between 50.0 - 100.0 s, and compared with the experimental data from the literature²², and given in Figure 2. The main exiting emissions compare reasonably well with the experimental data but as expected additional gaseous species and reaction models do not greatly influence the main exiting emissions due to the low concentrations. This is due to the amount of nitrogen and sulphur species present in the coal being much low than the remaining species so the concentration of NH_3 and H_2S available for the additional reactions is very low in comparison.

The impact of the inclusion of additional species and reactions on the computational time is considered. The simulations were carried out on the supercomputer, IRIDIS 3 at the University of Southampton. The maximum allocated time per session is a 60 hour period, therefore each case was allowed to run over four 60 hour periods and the simulation times achieved during these periods are given in Figure 3. Increasing the number of gaseous species slows the simulations with an approximate delay of 1.5-2.0 s in the simulation times between Cases 1 and 2. Case 3 included an additional two gaseous species and also an additional two reactions which incurs a more pronounced delay in the simulation. This is due to the additional computational requirements needed to perform the simulations. Slight variations can be seen between the achieved simulation times particularly in cases 2 and 3 where the initial runs took slightly longer to perform. The amount of time to reach convergence of each iteration influences the times achieved during the runs. In case 2 and 3 the bed contains very low concentration species and additional slow reaction rates, which are lowest in the initial stages. As the concentration of these species accumulate the convergence time for the iterations improves.

Calcination-only vs Desulphurisation model

Two three-dimensional simulations were considered: one simulating the calcination process alone and the second including the desulphurisation process. Figure 4 compares the average mole fraction of SO_2 leaving

the reactor over a 100.0 s period, between 50.0 s and 150.0 s, for the calcination-only and calcination plus desulphurisation model. As expected, there is a significant decrease in SO_2 emissions using the desulphurisation model compared to the calcination-only model due to the consumption of SO_2 to form CaSO_4 . The CaSO_4 distribution within the reactor, Figure 5, occupies the lower bed where O_2 concentrations are high to promote the desulphurisation reaction. Whilst the high density of CaSO_4 , compared to the char, could result in the segregation of the CaSO_4 to the base of the reactor it is more likely that the high levels in lower regions is a result of the increased temperature near the air inlet. These higher temperatures increase the desulphurisation reaction rate therefore producing higher concentrations locally.

The low volume fraction of the CaSO_4 is due to the limited availability of the reactant, SO_2 . The both the calcination-only and the desulphurisation cases the mole fraction of SO_2 is very low, because the bed consists of char and CaCO_3 alone with the coal being introduced through the fuel inlet only. Therefore the overall amount of sulphur which is released is collectively very low. In order to make a comparison with experimental data the simulation is re-run with coal present, $\alpha_{\text{coal}} = 0.1$, within the bed, in addition to its introduction through the fuel inlet. The experiments of Norman et al.³⁰ were performed in excess of 500.0-600.0 s as this was the time required for the SO_2 to reach a form of steady state. The present work performed the coal bed simulation to 800.0 s as we previously demonstrated that steady state conditions were achieved after approximately 400.0 s - 500.0 s on a 2D calcination-only case²⁶. The average mole fraction of SO_2 leaving the reactor are compared with the experimental data³⁰ in Table 5. The mole fraction of SO_2 has greatly increased compared to the present benchmark due to the increased coal presence within the bed. A similar order of magnitude to the experimental data is observed but variations in set up and operating conditions lead to an expected variation in overall value.

Influences on SO_2 production

The average mole fractions of exiting SO_2 were tracked over a 150.0 s period and shown in Figure 6. High peaks occur as large collections of SO_2 leave the reactor. This is especially seen in the calcination-only model around 20.0 s, 80.0 s and 125.0 s. Peaks occur for the desulphurisation model but with a lower mole fraction due to SO_2 consumption. SO_2 is produced during the oxidation of H_2S so an increase in either the local temperature or concentration of any of the reactants, H_2S or O_2 , could be responsible for these peaks. Figure 7 plots the mole fractions of SO_2 , O_2 , H_2S and the temperature distribution at 73.5 s and 74.0 s at height $y = 0.03\text{m}$ for the calcination-only model. An increase in SO_2 occurs between this period prior to the peak observed at 80.0 s in Figure 6. The changes in temperature and O_2 distributions between the two time periods are negligible but there is an increase in H_2S which is responsible for the dramatic increase in SO_2 .

The increase in H_2S could be due to numerical errors but it is worth considering the bed behaviour during this time period to be more conclusive. Figure 8 displays the contours of the mole fraction of H_2S across a

plane (displayed in Figure 8a) at $x = 0.01$ m which spans between $y = 0$ m and $y = 0.3$ m at 72.00 s, 73.50 s, 73.75 s and 74.00 s. The H_2S descends towards the air/steam inlet where O_2 is prevalent, thus accelerating reaction HM6, producing additional SO_2 .

Figure 9a-c displays iso-surfaces of the gas with a volume fraction of 0.75 at the times 72.00 s, 73.00 s and 74.00 s. Previously at 72.00 s, in Figure 8b), the H_2S resided near the coal inlet. It is clear from Figure 9a, this is due to the large bubble formation build up from devolatilisation products, including H_2S . The large bubble in the lower region was endogenously formed from the products of the heterogeneous reactions that dominate the lower bed regions. As the lower bubble rises it coalesces with the bubble near the coal inlet and continues up the bed, as shown at 73.00 s in Figure 9b,c. Devolatilisation products form a new bubble near the coal region however a slight downward tendency is apparent at 74.00 s.

The y-direction velocity distributions of the solid particles in Figure 9d-f show faster upward motion occurs in bubble regions where bed resistance is low. This explains why the H_2S remains high, near the coal inlet at 72.00 s, as the velocity vectors, in Figure 9d, have a positive velocity (indicating an upward direction) into the bubble. The velocities at 73.00 s and 74.00 s (Figure 9d,e) displays a strong downward motion transporting the local solids and gases, i.e., devolatilisation products, towards the base of the reactor. This downward motion occurs as the bed occupies the voidage left by the ascending bubbles. The motion of the bed greatly influences the reactions as the bed aids the transport of the reactants to areas where the reactions dominate, such as oxidation reactions near the air inlet.

Conclusion

A CFD model for a bubbling bed coal gasifier has been developed using one gaseous phase and five particulate phases. Compared to previous models which incorporated all the solid materials as a single phase this model allows for the simulation of realistic segregation effects due to the different properties. The inclusion of chemical reactions into an Eulerian-Eulerian framework is recent due to its complexity. The different stages of gasification were considered, namely, devolatilisation, heterogeneous and homogeneous reactions and limestone calcination between different phases. The desulphurisation process was also introduced to determine the model's capability of simulating low concentrations of species.

Assumptions are regularly made in CFD modelling regarding the accuracy of the chemical models and balancing acts are carried out between the inclusion of more detailed species to improve results and computational time/expense. The present results show that the inclusion of low concentration nitrogen and sulphur based species does not affect the emissions of the major species leaving the reactor as nitrogen and sulphur concentrations are so small in comparison to the major species. However, the CFD predictions of the major species agree well with the experimental data.

The inclusion of additional species and reactions incurs a computational overhead. On the other hand, the inclusion of sulphur and nitrogen in computational models is important as current research focuses on the reduction of SO_x and NO_x emissions to meet regulations. The present work shows that it is possible to carry out an Eulerian-Eulerian CFD model for multiple gaseous species with the newly incorporated reaction modelling for calcination and/or desulphurisation for fluidised bed technologies to aid future design optimisation.

Three-dimensional simulations were performed comparing SO_2 emissions from the calcination-only model and the calcination plus desulphurisation model. The average mole fraction of SO_2 leaving the reactor showed a decrease, as expected, using the desulphurisation model due to the additional consumption of SO_2 . Occasional high peaks of SO_2 were observed for both the calcination-only and the desulphurisation model, greater for the calcination-only case. This was due to the mixing behaviour of the fluidised bed distributing concentrated collections of reactants to higher temperature regions, thus accelerating the production of SO_2 . The occurrence frequencies and magnitudes of the peaks vary for both the calcination-only and calcination plus desulphurisation models, which indicates complex flow and reaction dynamics in the fluidised beds.

Future applications as a result of this work include the use of more accurate yield predictions for low concentration species and additional reactions between intermediate reactants to provide analyse of NO_x and SO_x formation in greater depth.

References

- [1] Berruti F, Chaouki J, Godfroy L, Pugsley T, Patience G. Hydrodynamics of circulating fluidized bed risers: a review. *Can J Chem Eng.* 1995;73(5):579–602.
- [2] Samuelsberg A, Hjertager B. An experimental and numerical study of flow patterns in a circulating fluidized bed reactor. *Int J Multiphase Flow.* 1995;22:575–591.
- [3] Benyahia S, Arastoopour H, Knowlton T, Massah H. Simulation of Particles and Gas Flow Behaviour in the Riser Section of a Circulating Fluidized Bed using the Kinetic Theory Approach for the Particulate Phase. *Powder Technol.* 2000;112:24–33.
- [4] Almuttahir A, Taghipour F. Computational fluid dynamics of high density circulating fluidized bed riser: Study of modeling parameters. *Powder Technol.* 2008;185:11–23.
- [5] Goldschmidt M, Kuipers J, van Swaaij W. Hydrodynamic modelling of dense gas-fluidized beds using the kinetic theory of granular flow: effect of restitution coefficient on bed dynamics. *Chem Eng Sci.* 2001;56:571.

- [6] Armstrong LM, Luo K, Gu S. Two-dimensional and Three-dimensional Computational Studies of Hydrodynamics in the Transition from Bubbling to Circulating Fluidised Bed. *Chem Eng J.* 2010;160:239–248.
- [7] Patil D, Smit J, van Sint Annaland M, Kuipers J. Wall-to-bed Heat Transfer in Gas-Solid Bubbling Fluidized Beds. *AIChE J.* 2006;52:58–74.
- [8] Schmidt A, Renz U. Numerical prediction of heat transfer in fluidized beds by a kinetic theory of granular flows. *Int J Therm Sci.* 2000;39:871–885.
- [9] Kuipers J, Prins W, van Swaaij W. Numerical calculation of wall-to-bed heat transfer coefficients in gas-fluidized beds. *AIChE J.* 1992;38:1079–1091.
- [10] Armstrong LM, Luo K, Gu S. CFD modelling of the gasification of coal particles in fluidised beds. In: *Proceedings of the International Heat Transfer Conference, Washington, DC, USA.* 2010; .
- [11] Ge W, Li J. Pseudo-particle approach to hydrodynamics of gas/solid two-phase flow. In: *Proceedings of the 5th International Conference on Circulating Fluidized Beds, Beijing: Science Press.* 1997; pp. 260–265.
- [12] Ge W, Li J. Macro-scale pseudo-particle modeling for particle-fluid systems. *Chin Sci Bulletin.* 2001; 46(18):1503–1507.
- [13] Ge W, Li J. Macroscale Phenomena Reproduced in Microscopic Systems-Pseudo-Particle Modeling of Fluidization. *Chem Eng Sci.* 2003;58:1565–1585.
- [14] Papadikis K, Bridgwater A, Gu S. CFD modelling of the fast pyrolysis of biomass in fluidised bed reactors, Part A: Eulerian computation of momentum transport in bubbling fluidised beds. *Chem Eng Sci.* 2008;63 (16):4218–4227.
- [15] Papadikis K, Gu S, Bridgwater A. CFD modelling of the fast pyrolysis of biomass in fluidised bed reactors. Part B: Heat, momentum and mass transport in bubbling fluidised beds. *Chem Eng Sci.* 2009; 64:1036–1045.
- [16] Andrews M, O’Rourke P. The multiphase particle-in-cell (MP-PIC) method for dense particulate flows. *Int J Multiphase Flow.* 1996;22:379–402.
- [17] Snider D. An Incompressible Three-Dimensional Multiphase Particle-in-Cell Model for Dense Particle Flows. *J Comput Phys.* 2001;170:523–549.
- [18] O’Rourke P, Zhao P, Snider D. A model for collisional exchange in gas/liquid/solid fluidized beds. *Chemical Engineering Science.* 2009;64:1784–1797.

- [19] Snider D, Clark S, O'Rourke P. Eulerian-Lagrangian method for three-dimensional thermal reacting flow with application to coal gasifiers. *Chem Eng Sci.* 2011;66:1285–1295.
- [20] Gidaspow D. *Multiphase flow and fluidization, continuum and kinetic theory descriptions.* Academic Press, Inc. 1994.
- [21] Yu L, Lu J, Zhang X, Zhang S. Numerical simulation of the bubbling fluidized bed coal gasification by the kinetic theory of granular flow (KTGF). *Fuel.* 2007;86:722–734.
- [22] Ocampo A, Arenas E, Chejne F, Espinel J, Londono C, Aguirre J, Perez J. An experimental study on gasification of Colombian coal in fluidised bed. *Fuel.* 2003;82:161–164.
- [23] Wang X, Jin B, Zhong W. Three-dimensional simulation of fluidized bed coal gasification. *Chem Eng Proc.* 2009;48:695–705.
- [24] Gerber S, Behrendt F, Oevermann M. An Eulerian modeling approach of wood gasification in a bubbling fluidized bed reactor using char as bed material. *Fuel.* 2010;89(10):2903–2917.
- [25] Armstrong LM, Luo K, Gu S. Effects of limestone calcination on the gasification processes in a BFB coal gasifier. *Chem Eng J.* 2011;168:848–860.
- [26] Armstrong LM, Luo K, Gu S. A parametric study of the gasification processes in a BFB coal gasifier. *Ind Eng Chem Res.* 2011;50:5959–5974.
- [27] de Souza-Santos M. Comprehensive modeling and simulation of fluidized bed boilers and gasifiers. *Fuel.* 1989;68:1507–1521.
- [28] Chejne F, Hernandez J. Modeling and simulation of coal gasification process in fluidized bed. *Fuel.* 2002;81:1687–1702.
- [29] Jones J, Harding A, Brown S, Thomas K. Detection of reactive intermediate nitrogen and sulfur species in the combustion of carbons that are models for coal chars. *Carbon.* 1995;33:833–843.
- [30] Norman J, Pourkashanian M, Williams A. Modelling the formation and emission of environmentally unfriendly coal species in some gasification processes. *Fuel.* 1997;76:1201–1216.
- [31] Shimizu T, Satoh M, Fujikawa T, Tonsho M, Inagaki M. Simultaneous reduction of SO₂, NO_x and N₂O emissions from a two-stage bubbling fluidized bed combustor. *Energy and Fuels.* 2000;14:862–868.
- [32] Ma R, Felder R, Ferrell J. Evolution of hydrogen sulfide in a fluidized bed coal gasification reactor. *Ind Eng Chem Res.* 1989;28:27–33.
- [33] Goyal A, Rehmat A. Modeling of a fluidised bed coal carbonizer. *Ind Eng Chem Res.* 1993;32:1396–1410.

- [34] Lin W, Bu J, Korbee R, Svoboda K, van den Bleek C. Modelling SO₂ and NO_x emissions in fluidized bed combustion of coal. *Fuel*. 1993;72:299–304.
- [35] Lun C, Savage S, Jeffrey D, Chepurin N. Kinetic Theories for Granular Flow: Inelastic Particles in Couette Flow and Slightly Inelastic Particles in a General Flow Field. *J Fluid Mech*. 1984;140:223–256.
- [36] Jenkins J, Savage S. A theory for the rapid flow of identical, smooth, nearly elastic, spherical particles. *J Fluid Mech*. 1983;130:187–202.
- [37] Schaeffer D. Instability in the Evolution Equations Describing Incompressible Granular Flow. *J Diff Equ*. 1987;66:19–50.
- [38] Gidaspow D, Bezburuah R, Ding J. Hydrodynamics of Circulating Fluidized Beds: Kinetic Theory Approach. In: *Proceedings of the 7th Fluidization Conference*. 1992; .
- [39] Wen Y, Yu Y. Mechanics of Fluidization. *Chem Eng Prog Symp Ser*. 1966;62:100.
- [40] Ergun S. Fluid Flow through Packed Columns. *Chem Eng Prog*. 1952;48(2):89–94.
- [41] Syamlal M, O'Brien T. Derivation of a drag coefficient from velocity-voidage correlation. In: *U.S. Dept. of Energy, Office of Fossil Energy, National Energy Technology Laboratory, Morgantown, West Virginia April*. 1987; .
- [42] Gunn D. Transfer of heat or mass to particles in fixed and fluidised beds. *Int J Heat Mass Transfer*. 1978;21:467–476.
- [43] Loison R, Chauvin R. Pyrolyse rapide du charbon. *Chimie et Industrie*. 1964;91:269.
- [44] Fine D, Slater S, Sarofim A, Williams G. Nitrogen in coal as a source of nitrogen oxide emission from furnaces. *Fuel*. 1974;53:120–128.
- [45] Ross I, Davidson J. The combustion of carbon particles in a fluidized bed. *Chem Eng Res Des*. 1982; 60a:108–114.
- [46] Hobbs M, Radulovic P, Smoot L. Modeling fixed-bed coal gasifiers. *AIChE J*. 1992;38:681–702.
- [47] Hurt R, Calo J. Semi-global intrinsic for char combustion modeling. *Combustion and Flame*. 2001; 125:1138–2114.
- [48] Silcox G, Kramlich J, Pershing D. A mathematical model for the flash calcination of dispersed CaCO₃ and Ca(OH)₂ particles. *Ind Eng Chem Res*. 1989;28:155–160.
- [49] Stanmore B, Gilot P. Review calcination and carbonation of limestone during thermal cycling for CO₂ sequestration. *Fuel Proc Tech*. 2005;86:1707–1743.

- [50] Adanez J, Gayan P, Grasa G, deDiego L, Armesto L, Cabanillas A. Circulating fluidized bed combustion in the turbulent regime: modelling of carbon combustion efficiency and sulphur retention. *Fuel*. 2001; 80:1405–1414.
- [51] Enwald H, Peirano E, Almstedt A, Leckner B. Simulation of the fluid dynamics of a bubbling fluidized bed experimental validation of the two-fluid model and evaluation of a parallel multiblock solver. *Chem Eng Sci*. 1999;54:311–328.
- [52] Johnson P, Jackson R. Frictional-collisional constitutive relations for granular materials, with application to plane shearing. *J Fluid Mech*. 1987;176:67–93.
- [53] Petersen I, Werther J. Experimental investigation and modeling of gasification of sewage sludge in the circulating fluidized bed. *Chem Eng Proc*. 2005;44(7):717–736.

List of Figure Captions

Figure 1: Schematic diagram of the experimental set up taken from the literature²².

Figure 2: Comparison of cases 1, 2 and 3 with the experimental data taken from the literature.

Figure 3: Simulation times (s) achieved during four 60 hour periods for the different cases with varying numbers of species and reactions.

Figure 4: Average mole fraction of SO_2 over a 100.0 s period for the calcination-only and desulphurisation model.

Figure 5: Volume fraction of CaSO_4 throughout the reactor.

Figure 6: Mole fraction of SO_2 leaving the reactor using a calcination-only model and a model with desulphurisation.

Figure 7: Mole fraction distributions of a) SO_2 b) O_2 , c) H_2S and d) the temperature distribution across the reactor at $y = 0.03$ m at 73.5 s and 74.0 s.

Figure 8: Mole fraction of H_2S shown across the a) plane sliced at $x = 0.01$ m up to $y = 0.3$ m at the times b) 72.00 s, c) 73.50 s, d) 73.75 s and e) 74.0 s.

Figure 9: Iso-surface with gas volume fraction set to 0.75 (a - c) and the y-direction velocity distribution for the solids (d - f) at 72.00 s, 73.00 s and 74.00 s, respectively.

Figures

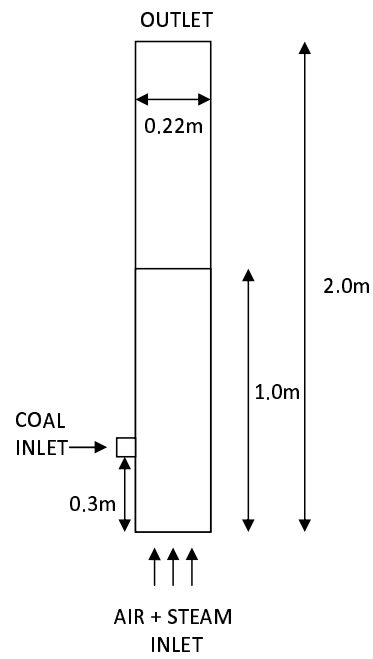


Figure 1: Schematic diagram of the experimental set up taken from the literature²².

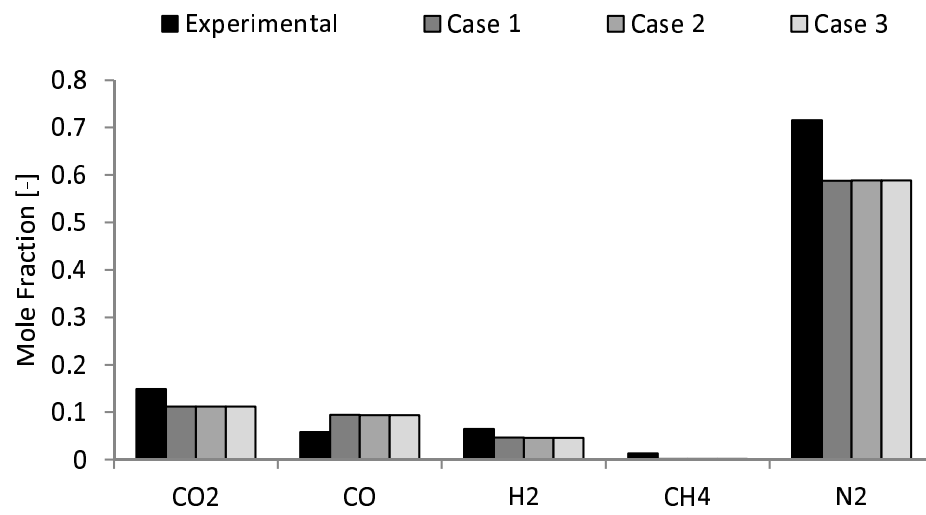


Figure 2: Comparison of cases 1, 2 and 3 with the experimental data taken from the literature.

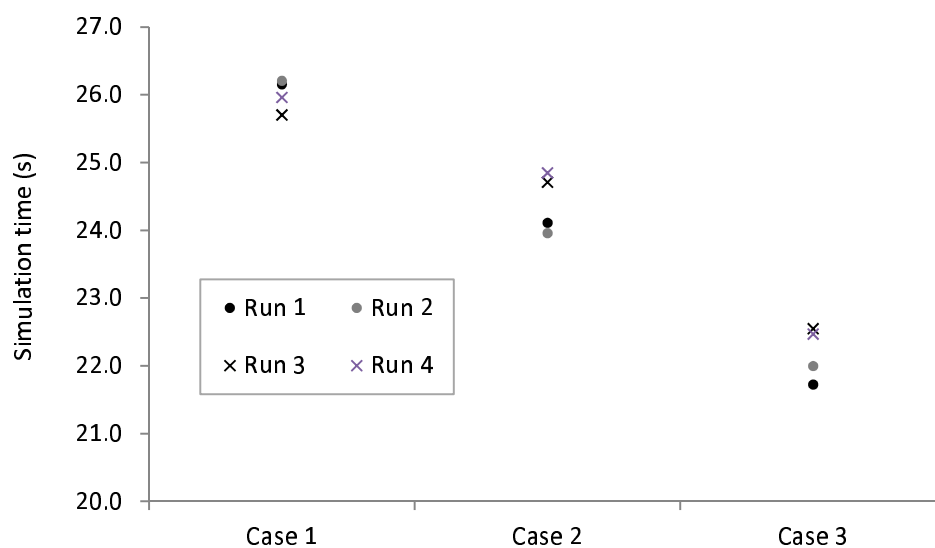


Figure 3: Simulation times (s) achieved during four 60 hour periods for the different cases with varying numbers of species and reactions.

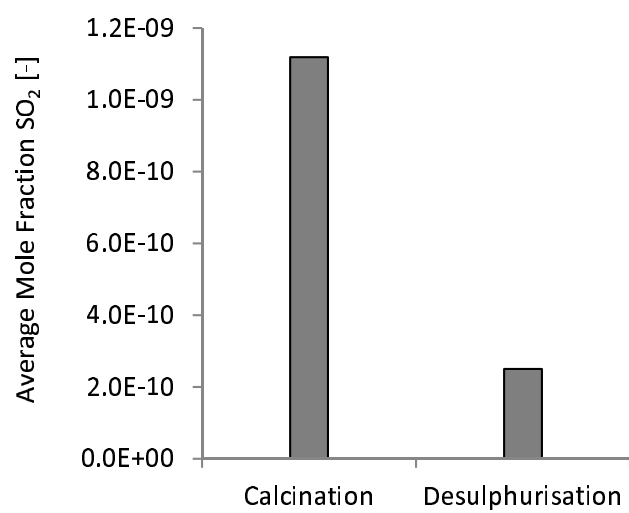


Figure 4: Average mole fraction of SO₂ over a 100.0 s period for the calcination-only and desulphurisation model.

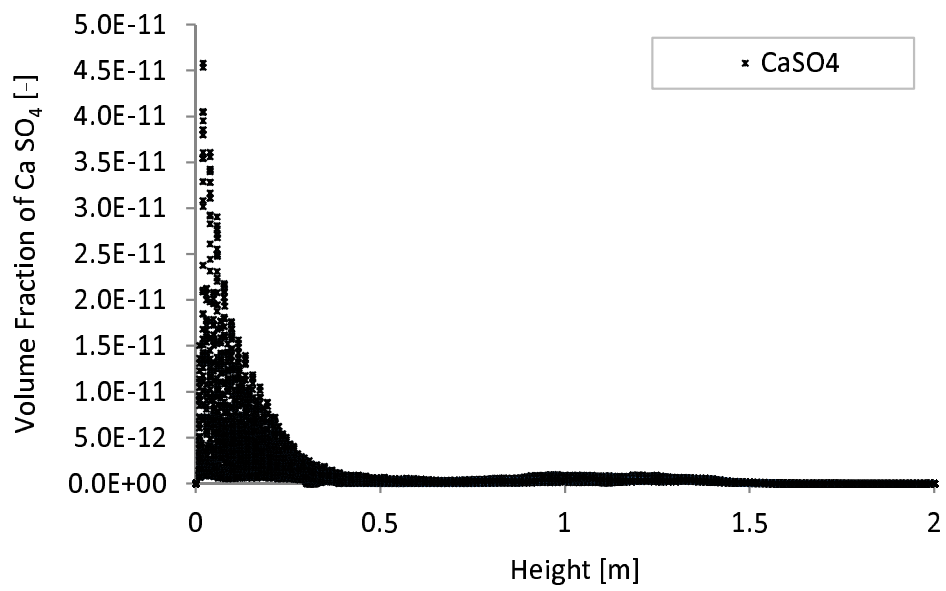


Figure 5: Volume fraction of CaSO_4 throughout the reactor.

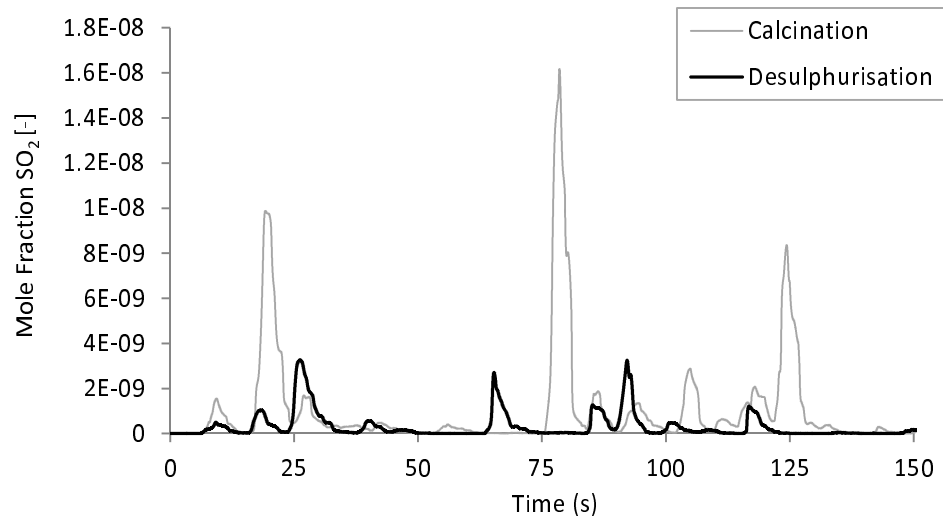


Figure 6: Mole fraction of SO₂ leaving the reactor using a calcination-only model and a model with desulphurisation.

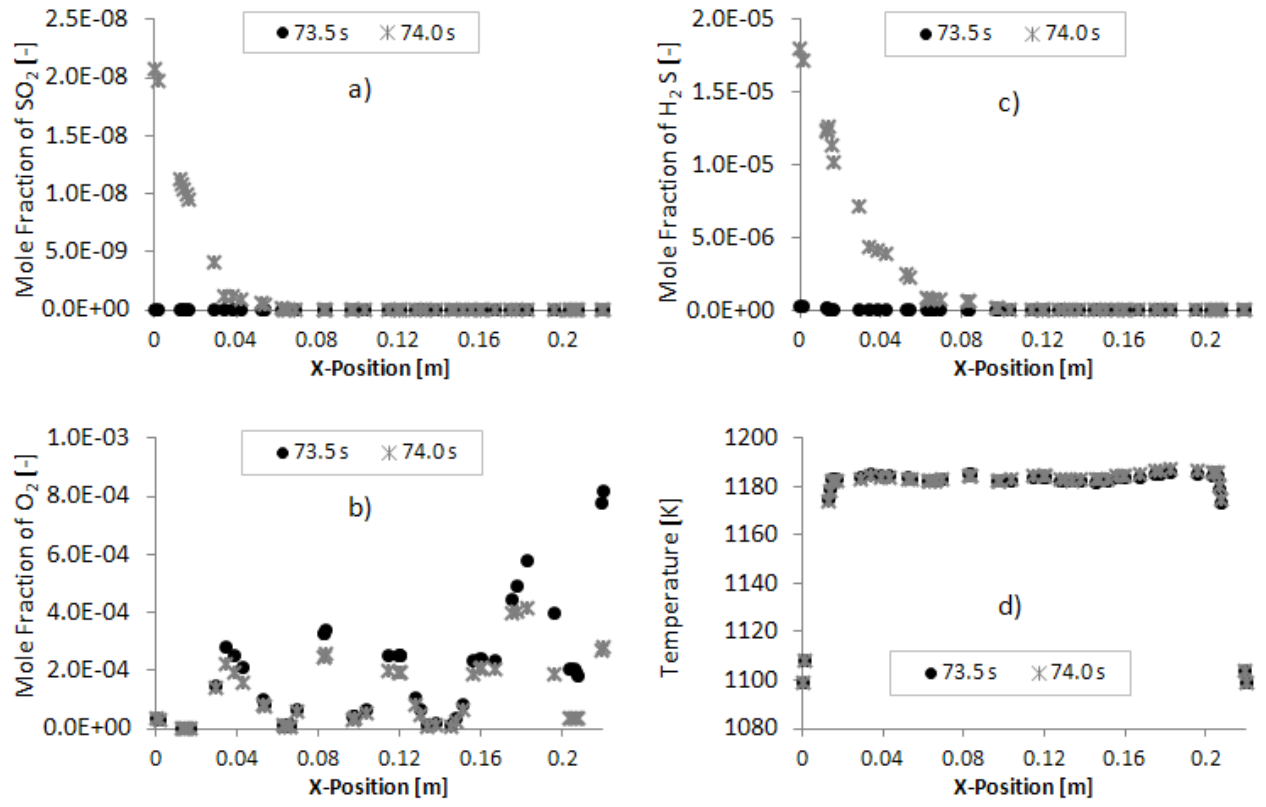


Figure 7: Mole fraction distributions of a) SO_2 b) O_2 , c) H_2S and d) the temperature distribution across the reactor at $y = 0.03$ m at 73.5 s and 74.0 s.

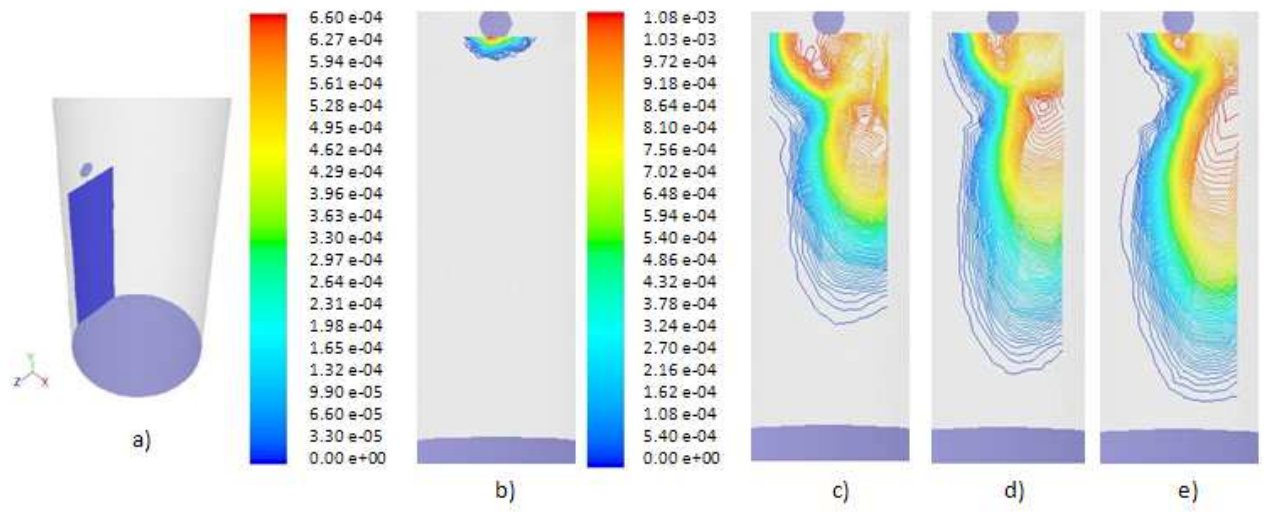


Figure 8: Mole fraction of H_2S shown across the a) plane sliced at $x = 0.01$ m up to $y = 0.3$ m at the times b) 72.00 s, c) 73.50 s, d) 73.75 s and e) 74.0 s.

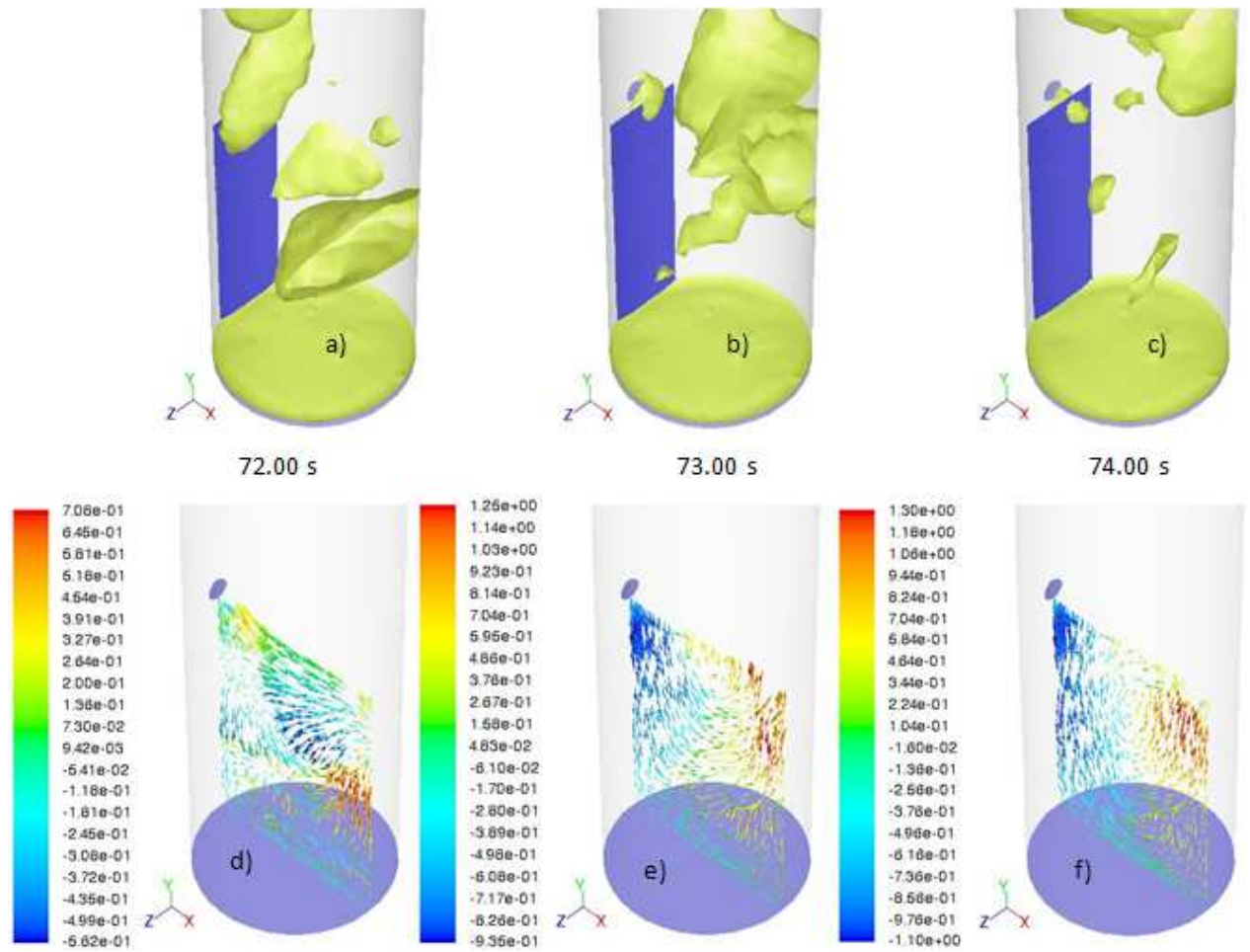


Figure 9: Iso-surface with gas volume fraction set to 0.75 (a - c) and the y-direction velocity distribution for the solids (d - f) at 72.00 s, 73.00 s and 74.00 s, respectively.

Tables

Table 1: Heterogeneous, homogeneous, calcination & desulphurisation reactions with their kinetic rate constants.

	Heterogeneous	Kinetic Rate Constants	Ref
HT1	$C + O_2 \rightarrow CO_2$	$K_{Arr1} = 1.04 \times 10^5 T_c \exp\left(\frac{-11200}{T_c}\right)$	45,46
HT2	$C + H_2O \rightarrow CO + H_2$	$K_{Arr2} = 342 T_c \exp\left(\frac{-15600}{T_c}\right)$	45,46
HT3	$C + CO_2 \rightarrow 2CO$	$K_{Arr3} = 342 T_c \exp\left(\frac{-15600}{T_c}\right)$	45,46
HT4	$C + 2H_2 \rightarrow CH_4$	$K_{Arr4} = 3.42 \times 10^{-3} \exp\left(\frac{-15600}{T_c}\right)$	45,46
Homogeneous			
HM1	$CO + 0.5O_2 \rightarrow CO_2$	$K_1 = 1.0 \times 10^{15} \exp\left(\frac{-16000}{T_g}\right) C_{CO} C_{O_2}^{0.5}$	28,47
HM2	$H_2 + 0.5O_2 \rightarrow H_2O$	$K_2 = 5.159 \times 10^{15} \exp\left(\frac{-3430}{T_g}\right) T^{-1.5} C_{H_2}^{1.5} C_{O_2}$	28,47
HM3	$CH_4 + 2O_2 \rightarrow 2H_2O + CO_2$	$K_3 = 3.552 \times 10^{14} \exp\left(\frac{-15700}{T_g}\right) T^{-1} C_{CH_4} C_{O_2}$	28,47
HM4	$CO + H_2O \rightleftharpoons H_2 + CO_2$	$K_4 = 2780 \exp\left(\frac{-1510}{T_g}\right) \left[C_{CO} C_{H_2O} - \frac{C_{CO_2} C_{H_2}}{0.0265 \exp(3968/T_g)} \right]$	28,47
HM5	$4NH_3 + 5O_2 \rightarrow 4NO + 6H_2O$	$K_5 = 9.78 \times 10^{11} \exp\left(\frac{-19655}{T_g}\right) C_{NH_3}^{0.86} C_{O_2}^{1.04}$	28,47
HM6	$2H_2S + 3O_2 \rightarrow 2SO_2 + 2H_2O$	$K_6 = 9.78 \times 10^{11} \exp\left(\frac{-19655}{T_g}\right) C_{H_2S}^{0.86} C_{O_2}^{1.04}$	28,47
Calcination			
CAL	$CaCO_3 \rightarrow CaO + CO_2$	$K_{cal} = 1.22 \exp(-4026/T_l)$	48
Desulphurisation			
DES	$CaO + SO_2 + 0.5O_2 \rightarrow CaSO_4$	$K_{ds} = 470 \exp(-8812.13/T_l) S_g \lambda_l$	50

Table 2: Characteristics of solids.

Coal Properties					
<i>Proximate Analysis (wt%)</i>					
Moisture	2.6				
Volatile matter	41.8				
Fixed carbon	54.1				
Ash	1.5				
<i>Ultimate Analysis (wt%)</i>					
Carbon	75.3				
Hydrogen	5.4				
Oxygen	15.6				
Nitrogen	1.8				
Sulphur	0.4				
Ash	1.5				
<i>Others</i>	<i>Coal</i>	<i>Char</i>	<i>CaCO₃</i>	<i>CaO</i>	<i>CaSO₄</i>
Mean particle size(mm)	0.62	0.60	0.60	0.60	0.60
Apparent density (kg/m ³)	1250	450	2700	3320	2960
High heating value (kJ/kg)	29695				

Table 3: Operating conditions and experimental results.

Operating Conditions		Experimental results	
Air (kg/h)	28.4	H ₂ (%)	6.48
Steam (kg/h)	4.6	CO ₂ (%)	14.86
Coal (kg/h)	8.0	N ₂ (%)	71.54
Limestone (kg/h)	0.8	CH ₄ (%)	1.29
Entrance temp (K)	641.15	CO (%)	5.80
Reactor temp (K)	1099.15		

Table 4: Two-dimensional cases with varying combinations of gas species and reactions.

Case	Gas Species	#
1	H ₂ O, O ₂ , CO ₂ , CO H ₂ , CH ₄ , C ₆ H ₆ , N ₂	8
2	H ₂ O, O ₂ , CO ₂ , CO H ₂ , CH ₄ , C ₆ H ₆ , N ₂ , NH ₃ , H ₂ S	10
3	H ₂ O, O ₂ , CO ₂ , CO H ₂ , CH ₄ , C ₆ H ₆ , N ₂ , NH ₃ , H ₂ S, NO, SO ₂	12
Case	Activated Homogeneous Reactions	#
1	HM1, HM2, HM3, HM4	4
2	HM1, HM2, HM3, HM4	4
3	HM1, HM2, HM3, HM4, HM5, HM6	6
Case	Activated Heterogeneous Reactions	#
1	HT1, HT2, HT3, HT4	4
2	HT1, HT2, HT3, HT4	4
3	HT1, HT2, HT3, HT4	4

Table 5: SO₂ yields comparing a simulated bed of coal against experimental data from the literature³⁰.

Case	Mole fraction of SO₂
Present case	6.157710^{-3}
Published case	$\approx 9.7710^{-3}$

Nomenclature

Greek Letters

α_i	Volume fraction
γ_i	Collisional dissipation of energy, W/mK
κ	Turbulent kinetic energy, m ² /s ²
λ_i	Thermal conductivity of species, W/m ² K
μ_i	Shear viscosity, kg/s m
ϕ	Angle of internal friction, °, Eq. (15)
ρ_i	Density, kg/m ³
σ_κ	Turbulent Prandtl numbers for κ
σ_ε	Turbulent Prandtl numbers for ε
τ_i	Stress tensor, Pa
Θ_s	Particle phase pseudo-temperature, m/s ²
v_i	Velocity, m/s
ε	Dissipation rate of turbulent kinetic energy, m ² /s ³
ξ_i	Bulk viscosity, kg/s m

Symbols

t	Time, s
$\bar{\bar{I}}$	Stress tensor, Pa
C_D	Drag coefficient
C_i	Concentration of species i , kmol/m ³
C_p	Specific heat, J/kgK
d_s	Particle diameter, m
D_i	Diffusion coefficient for species, m ² /s
e	Coefficient of restitution

g	Gravity, m/s ²
g_0	Radial distribution function
G_κ	Shear production
H	Specific enthalpy, J/kg
h	Heat transfer coefficient, W/m ² K
J_i	Diffusion flux of species i , kg/m ² s
k_{Θ_s}	Diffusion coefficient for granular energy, kg/ms
K_{Arr}	Kinetic rate constant
K_{Dif}	Diffusion rate constant
K_i	Drag, kg/m ³ s
p	Gas pressure, Pa
p_i	Phase pressure, Pa
Q_i	Intensity of heat exchange between phases, W/m ²
R	Universal gas constant, J/kmol K
$R_{g,i}$	Net rate of production of homogeneous species i
$R_{s,i}$	Heterogeneous reaction rate
S_i	Mass source term, kg/m ³ s
T	Temperature, K
w_i	Species molecular weight, kg/kmol
X_i	Molar fraction of species
Y_i	Mass fraction of species
<i>Subscripts</i>	
g	Gas phase
i	General Index, i th species
q	Phase

s Solids phase

w Wall

c Char

g_l Gas laminar flow

g_t Gas turbulent flow

Dimensionless Numbers

Nu Nusselt number

Pr Prandtl number

Re Reynolds number

Sc_t Turbulent Schmidt number

Sh Sherwood number

Multifluid modeling of the desulfurization process within a bubbling fluidized bed coal gasifier

Armstrong, L-M.

2013-06-01T00:00:00Z

L.M. Armstrong, S. Gu, K.H. Luo. Multifluid modeling of the desulfurization process within a bubbling fluidized bed coal gasifier. AIChE Journal, 2013, Vol. 59, No. 6, pp1952-1963

<http://dx.doi.org/10.1002/aic.13997>

Downloaded from CERES Research Repository, Cranfield University